Development and Test of Hydrostatic Extraction Scheme in Spectral Model①

Zhang Daomin (张道民) *Sheng Hua* (盛 华) and *Ji Liren* (纪立人)
Institute of Atmospheric Physics, Academia Sinica, Beijing 100080
Received July 31, 1989

ABSTRACT

The introduction of "hydrostatic extraction" scheme, or "standard stratification approximation", into spectral model gained some advantages compared with commonly used schemes. However, computational instability may occur for high vertical resolution versions if the stratification parameter C_0 taken as a constant. In this paper, the possible cause leading to the instability is discussed and an improved scheme presented where C_0 is generalized to be a function of both height and latitudes. Hence the reference atmosphere gets closer to the real atmosphere and the temperature deviation field to be expanded becomes smoother everywhere. Test by real case forecasts shows good computational stability of the new scheme and better prediction performance than-usual schemes of spectral model.

I. INTRODUCTION

The "hydrostatic extraction" scheme , or standard stratification approximation, posed by Zeng(1979) has been introduced into spectral model by Chen et al(1987). The essence of the scheme is to introduce a reference atmosphere and the spectral expansion is conducted only for the deviation of prognostic variables, i. e. the difference between the real and reference atmosphere, thus improving the convergence rate of the expansion. Apparently, the closer the reference state approaches to the real and the smoother the deviation field, the better the effect. The reduction of truncation error of the spectral expansion not only improves the calculation of pressure gradient term in sigma coordinates but also alleviates those problems such as negative orography and Gibbs phenomenon of spectral models. The scheme has been tested by time integration using Rossby– Haurwitz waves and real cases. The result shows better performance of the scheme than ordinary ones when the vertical resolution of the model being low.

However, the parameter C_0 depicting the stratification of the reference atmosphere is taken as constant in their scheme, which implies that only a slight change of temperature lapse rate is allowed (the value at 10 hPa remains more than half of that at 1000 hPa). As a result, there is considerable difference of temperature between the reference state and the real at the middle and upper stratosphere. The accuracy of the scheme is reduced with the increase of levels in the vertical, when the horizontal truncated wave number is fixed (T21). For a seven–level version, the time integration of the model remains normal. But for a nine–level version, the computational instability occurs at 51–hr of integration (for June 14, 1979 case). If the resolution is increased up to 15 levels, only 33–hr stable integration is possible.

①This work has been carried out under the support of the Medium–range Numerical Weather Forecast research project.

To cope with this problem, a referene atmosphere with varying lapse rate, i. e. C_0 being a function of pressure p is first introduced into the model, which overcomes the computational instability and achieves better results. As a step further, the scheme has been generalized with a height and latitude dependent C_0 so as to make the reference state more realistic. The development of C_0 from a constant to a function of both height and latitude, which can be updated by each initial field, is a natural and important generation of the "hydrostatic extraction" scheme.

In the following, Section II will give a detailed discussion on various model reference atmosphere. In Section III the model governing equations are deduced. For comparison under different conditions, the model has been designed with option in vertical and horizontal resolution, and in global and hemispheric versions. In Section IV using several real cases, the extraction scheme is tested and examined under various conditions, focusing mainly on T42L9 version. Finally some conclusions are given in the last section.

II. COMPARISON OF VARIOUS REFERENCE ATMOSPHERE

In the hydrostatic extraction method, the stratification parameter C_0 presenting the reference atmospheric state is introduced into the model, it is defined as

$$\frac{R^2\bar{T}}{g}\left(\frac{g}{C_p}+\frac{d\bar{T}}{dz}\right)=C_0^2\ , \tag{2.1}$$

where $\bar{T}$ is the temperature of reference atmosphere. Obviously, for different reference atmosphere, there exists corresponding C_0. Fig.1 shows the change of C_0 with height which is calculated from average temperature over Northern Hemisphere for four cases representing

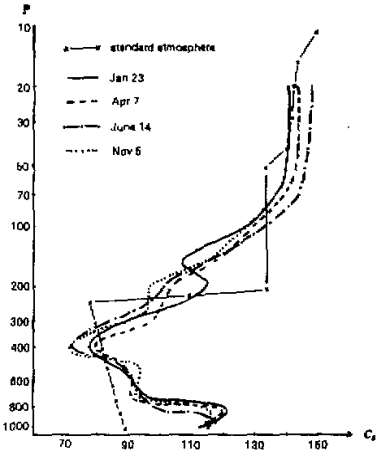

Fig.1. Variation of C_0 with height for real cases and standard atmosphere over Northern Hemisphere. (The ordinate is in $\ln P$ scale, the same for Fig.3, Fig.8 and Fig.9).

various seasons (they are April 7,June 14,November 5 and January 23 respectively). C_0 calculated by the standard atmospheric temperature of America (1976) is shown in Fig.1 as well. As can be seen from Fig.1, C_0 not only changes with height but also with time. Abrupt change of atmospheric temperature near the tropopause makes C_0 have a minimum beneath

the tropopause. C_0 calculated from standard atmosphere is 88.8m / s near the surface, and decreases upwards to be 78m / s near 245 hPa. There exists an isothermal layer from about 230 to 55 hPa, so C_0 increases abruptly to 133 m / s near 230 hPa and keeps constant in the layer, then rises slowly upwards from 55 hPa.

1. *C_0 Being a Constant*

Assume that the reference atmosphere satisfies the hydrostatic equation

$$\frac{\partial \overline{\varphi}}{\partial \ln P} = -R\overline{T}. \tag{2.2}$$

If C_0 is taken as constant, from Eqs. (2.1)–(2.2), the temperature and geopotential height of reference atmosphere at any pressure surface can be derived as follows:

$$\overline{T}(p) = \frac{C_p C_0^2}{R^2} + \left(\overline{T}_0 - \frac{C_p C_0^2}{R^2}\right)\left(\frac{P}{P_0}\right)^{R/C_p} \tag{2.3}$$

$$\overline{\varphi}(p) = \frac{C_p}{R}\left(R\overline{T}_0 - \frac{C_p C_0^2}{R}\right)\left[1 - \left(\frac{P}{P_0}\right)^{R/C_p}\right] - \frac{C_p C_0^2}{R}\ln\left(\frac{P}{P_0}\right), \tag{2.4}$$

where $\overline{T}_0$ and P_0 are the temperature and pressure at sea level under standard condition respectively. $\overline{T}_0$ is taken as 288K, P_0 1013 hPa. The temperature T and geopotential height of the model atmosphere are then separated into those of the reference atmosphere and the deviation from it

$$T(\lambda,\mu,p,t) = \overline{T}(p) + T'(\lambda,\mu,p,t)$$
$$\varphi(\lambda,\mu,p,t) = \overline{\varphi}(p) + \varphi'(\lambda,\mu,p,t). \tag{2.5}$$

Taking C_0=88.8 m / s in Chen Jiabin et al.(1987), it approximates the values under 250 hPa in standard atmosphere. The vertical temperature profile of the reference atmosphere calculated by (2.3) varies linearly with ln$P$. The temperature deviations T' of the model atmosphere below 250 hPa are not large. For example, T' averaged over the Northern Hemisphere is not larger than 15°C below 250 hPa for June 14 case (Fig.2). But it reaches 80 as large at 10 hPa.

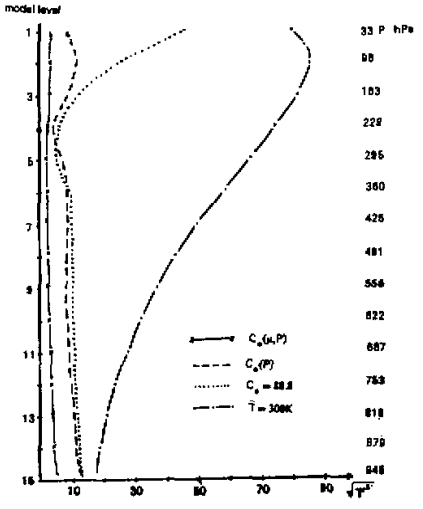

Fig.2 Initial temperature deviation averaged over the Northern Hemisphere (for June 14 case).

2. C_0 Changing with Height

As shown in Fig.1, it is more reasonable to take $C_0 = C_0(p)$, the temperature obtained from $C_0(p)$ corresponding to the observed in which the temperature decreases with height in the troposphere and increases in the stratosphere. Assuming $C_0 = C_0(p)$, Eq.(2.1) becomes

$$\frac{R^2\overline{T}}{g}\left(\frac{g}{C_p}+\frac{d\overline{T}}{dz}\right)=C_0^2(p). \tag{2.6}$$

And Eqs.(2.3)–(2.4) can be written in the following recurrence form

$$\overline{T}_k(P_k)=\frac{C_pC_k^2}{R^2}+\left(\overline{T}_{k+1}-\frac{C_pC_k^2}{R^2}\right)\left(\frac{P_k}{P_{k+1}}\right)^{R/C_p} \tag{2.7}$$

$$\overline{\varphi}(P_k)=\overline{\varphi}_{k+1}(P_{k+1})+\frac{C_p}{R}\left(R\overline{T}_{k+1}-\frac{C_pC_k^2}{R}\right)\left[1-\left(\frac{P_k}{P_{k+1}}\right)^{R/C_p}\right]$$
$$-\frac{C_pC_k^2}{R}\ln\left(\frac{P_k}{P_{k+1}}\right). \tag{2.8}$$

The governing equations for spectral model are the same as given by Chen et al.(1987) except for C_0 changing with height. C_0 (namely C_k) may be calculated by standard atmosphere (Zhang Xuehong,1990) or by initial data, and the temperature deviations T' obtained by the latter are even smaller, only about 10°C as shown in Fig.2.

3. C_0 Being a Function of Both Height and Latitude

As is well known, the vertical temperature profile of real atmosphere not only changes with height, but also with latitude (see Fig.3). The tropopause is about 100 hPa near the equatorial region, but about 400 hPa at high latitude region. $C_0(p)$ calculated by standard atmosphere or real data represents the state in the mid–latitude area, while the temperature deviation is still larger at low or high latitudes. It is better to take into account the variation of C_0 with height and latitude, namely $C_0 = C_0(\mu,p)$, which is a natural generalization of $C_0 = C_0(p)$. The initial temperature deviation field becomes smaller everywhere when C_0 being taken as $C_0(\mu,p)$. For June 14 case, maximum mean deviation over the Northern Hemisphere is not greater than 5°C (Fig.2). $C_0(\mu,p)$, like $C_0(p)$, may be calculated by standard atmosphere or by initial data. Considering the tropopause also changing with time, the $C_0(\mu,p)$ obtained by real initial data should be more realistic. In this case, formulations (2.6)–(2.8) are not changed, as long as the variables in the formulations are taken the function of both height and latitude. However, divergence and thermodynamic equation differ from those in Chen et al.(1987), which will be given in next section.

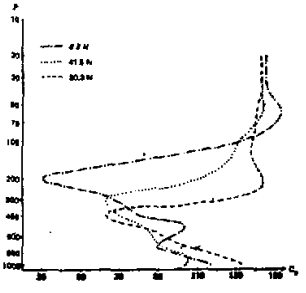

Fig.3. Change of C_0 with height at various latitudes(June 4, 1979 case).

III. GOVERNING EQUATIONS

Now we give the governing equations for spectral model when C_0 equals $C_0(\mu,p)$. The temperature T and geopotential height φ are separated into those of the reference state and the deviation from it as shown in Eq.(2.5), in which variables $\overline{T}$ and $\overline{\varphi}$ satisfy the hydrostatic equation (2.2). Assuming

$$\frac{R^2\overline{T}}{g}\left(\frac{g}{C_p}+\frac{d\overline{T}}{dz}\right)=C_0^2(\mu,P), \tag{3.1}$$

it can easily be verified that

$$\frac{\partial\overline{\varphi}}{\partial\lambda}+R\overline{T}\frac{\partial lnP_*}{\partial\lambda}=0 \tag{3.2}$$

$$\frac{\partial\overline{\varphi}}{\partial\mu}+R\overline{T}\frac{\partial lnP_*}{\partial\mu}\neq 0\ . \tag{3.3}$$

Horizontal momentum equations can be written as follows:

$$\frac{\partial U}{\partial t}=-\frac{U}{a(1-\mu^2)}\frac{\partial U}{\partial\lambda}-\frac{V}{a}\frac{\partial U}{\partial\mu}-\dot{\sigma}\frac{\partial U}{\partial\sigma}+fV-\frac{1}{a}\left(\frac{\partial\varphi'}{\partial\lambda}+RT'\frac{\partial lnP_*}{\partial\lambda}\right) \tag{3.4}$$

$$\frac{\partial V}{\partial t}=-\frac{U}{a(1-\mu^2)}\frac{\partial V}{\partial\lambda}-\frac{V}{a}\frac{\partial V}{\partial\mu}-\dot{\sigma}\frac{\partial V}{\partial\sigma}-fU-\frac{U^2+V^2}{a(1-\mu^2)}\mu-\frac{(1-\mu^2)}{a}\left(\frac{\partial\varphi'}{\partial\mu}+RT'\frac{\partial lnP_*}{\partial\mu}\right)-\frac{(1-\mu^2)}{a}\left(\frac{\partial\overline{\varphi}}{\partial\mu}+R\overline{T}\frac{\partial lnP_*}{\partial\mu}\right) \tag{3.5}$$

They are transformed into the vorticity and divergence equation again

$$\frac{\partial\zeta}{\partial t}=\frac{1}{a(1-\mu^2)}\frac{\partial F'_v}{\partial\lambda}-\frac{1}{a}\frac{\partial F_u}{\partial\mu} \tag{3.6}$$

$$\frac{\partial D}{\partial t}=\frac{1}{a(1-\mu^2)}\frac{\partial F_u}{\partial\lambda}+\frac{1}{a}\frac{\partial F'_v}{\partial\mu}-\nabla^2\left[\frac{U^2+V^2}{2(1-\mu^2)}+\varphi'\right], \tag{3.7}$$

where

$$F_u=V\cdot\zeta-\dot{\sigma}\frac{\partial U}{\partial\sigma}-RT'\frac{\partial\ln P_*}{a\partial\lambda}$$

$$F'_v=F_v-\frac{(1-\mu^2)}{a}\left(\frac{\partial\overline{\varphi}}{\partial\mu}+R\overline{T}\frac{\partial\ln P_*}{a\partial\mu}\right)$$

$$=-U\cdot\zeta-\dot{\sigma}\frac{\partial V}{\partial\sigma}-RT(1-\mu^2)\frac{\partial\ln P_*}{a\partial\mu}-(1-\mu^2)\frac{\partial\overline{\varphi}}{a\partial\mu}$$

$$U=u\cos\theta,\quad V=v\cos\theta,\quad \mu=\sin\theta.$$

They are different from those in Chen et al. (1987) in which the new term $\frac{(1-\mu^2)}{a}\left(\frac{\partial\overline{\varphi}}{\partial\mu}+R\overline{T}\frac{\partial\ln P_*}{\partial\mu}\right)$ is added in nonlinear term F'_ν.

The thermodynamic equation is as follows:

$$\frac{dT}{dt}-\frac{RT\omega}{C_pP}=0.$$

Substituting the first formula in (2.5) into the above equation we have

$$\frac{dT'}{dt}-\frac{RT'\omega}{C_pP}+\frac{d\overline{T}}{dt}-\frac{R\overline{T}\omega}{C_pP}=0.$$

Utilizing (3.1), the thermodynamic equation becomes

$$\frac{\partial T'}{\partial t}=\frac{1}{a(1-\mu^2)}\frac{\partial}{\partial\lambda}(UT')-\frac{1}{a}\frac{\partial}{\partial\mu}(VT')+$$
$$DT'-\dot{\sigma}\frac{\partial T'}{\partial\sigma}+\left(\frac{C_0^2}{R}+\frac{R}{C_p}T'\right)\frac{\omega}{P}-$$
$$\frac{V}{a}\left[\frac{\partial\overline{T}}{\partial\mu}-\left(\frac{R\overline{T}}{C_p}-\frac{C_0^2}{R}\right)\frac{\partial\ln P_*}{\partial\mu}\right]. \tag{3.8}$$

Comparing with the corresponding equation in Chen et al. (1987),there is an additional term in Eq (3.8), i.e. $\frac{V}{a}\left[\frac{\partial\overline{T}}{\partial\mu}c\left(\frac{R\overline{T}}{C_p}-\frac{C_0^2}{R}\right)\frac{\partial\ln P_*}{\partial\mu}\right]$. The other equations, such as tendency and hydrostatic equation, are the same as in Chen et al., i. e.

$$\frac{\partial(\ln P_*)'}{\partial t}=-\int_0^1 D+\nabla\cdot\nabla\ln P_*\,d\sigma \tag{3.9}$$

$$\frac{\partial\varphi'}{\partial\ln\sigma}=-RT'. \tag{3.10}$$

In order to ensure conservation of total energy, the term of energy transformation is written in the following form

$$\frac{\omega}{P}=\nabla\cdot\nabla\ln P_*-\frac{d\ln\sigma}{d\sigma}\int_0^\sigma(D+\vec{V}\cdot\nabla\ln P_*)d\sigma, \tag{3.11}$$

vertical speed in σ coodinates is written as

$$\dot{\sigma}=\sigma\int_0^1(D+\vec{V}\cdot\nabla\ln P_*)d\sigma-\int_0^\sigma(D+\vec{V}\cdot\nabla\ln P_*)d\sigma. \tag{3.12}$$

Equations (3.6)–(3.10) form a complete set of governing equations for adiabatic spectral model. The main difference between them and the equations in Chen et al. are that C_0 changes with both height and latitude and there are some new terms in vorticity, divergence and thermodynamic equation, which result from the change of the reference atmosphere with latitude. These new terms may be calculated on σ surface or on P surface. The vertical finite difference and spectral expansion are the same as in Chen et al..

IV. COMPARISON BETWEEN COMPUTATIONAL RESULTS OF DIFFERENT SCHEMES

Some real cases are predicted using the three versions of hydrostatic extraction, i.e. C_0 =constant (called IAPGSM1 hereafter), $C_0=C_0(p)$ (IAPGSM2) and $C_0=C_0(\mu,p)$ (IAPGSM3) and by usual spectral scheme (ECGSM) (Baede et al.,1980). In order to save

computer time, the integration is carried out only for the Northern Hemispheric model.

1. *Comparison of Results for Lower Resolution T21*

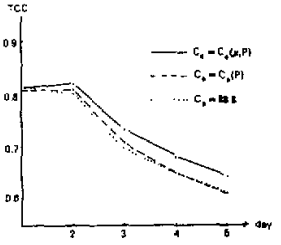

Fig.4. 500 hPa TCC predicted using T21L5 for different reference atmosphere (June 14,1979).

First of all, we give the forecast results up to 5 days in lower vertical resolution for June 14 case. Fig.4 shows the tendency correlation coefficients (TCC) of forecast height field at 500 hPa with T21L5. It can be seen that the forecast of three schemes is roughly the same for day 1, while the TCC of scheme IAPGSM3 is higher than the IAPGSM1 for the rest, about 3% higher a day for the last three days in average. The TCC of IAPGSM2 is higher than IAPGSM1 too for day 2 and day 3. They are equivalent for the last two days. This shows better prediction effect by both IAPGSM2 and IAPGSM3, especially the latter, than IAPGSM1. On the other hand, it also indicates that the scheme IAPGSM1 is useful when vertical resolution being lower. However, as mentioned above, its computational accuracy decreases with increasing vertical resolution. Computational instability appears when vertical levels are increased to 15 and integration is performed to 33 hours, while the other two schemes all normally run up to five days.

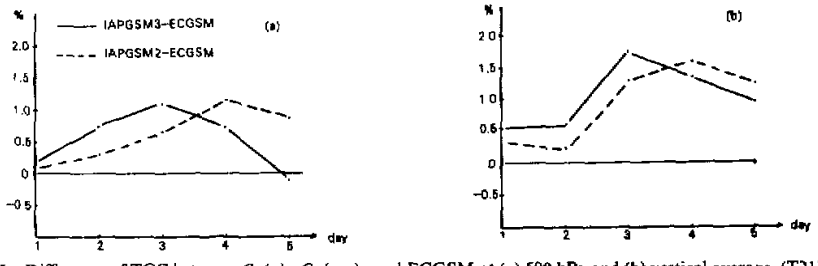

Fig.5. Difference of TCC between $C_0(p)$, $C_0(\mu,p)$ and ECGSM at (a) 500 hPa and (b) vertical average. (T21L15, April 7 case).

Next,we compare the forecasts of both IAPGSM2 and IAPGSM3 with ECGSM in high vertical resolution (15 levels) for April 7 case. We do the numerical integration up to 5 days using version T21L15, and give TCC and RMSE (root– mean– square error) of forecast height field at 500 hPa and that for vertical average (namely averaged for 100, 200, 300, 500, 700 and 850 hPa), respectively. It can be seen from Fig. 5 that vertical average of TCC for extraction scheme is 1.0% per day higher than ECGSM through forecast; and 500 hPa TCC is higher than ECGSM except for day 5. The superiority of hydrostatic extraction seems to reduce when vertical levels increase from 9 to 15. The possible reason is as follows. One of the advantages for hydrostatic extraction method lies in that $\partial\overline{T}/\partial P$ can be calculated in high

Table 1. TCC and RMSE of Height Field Predicted by IAPGSM3 and ECGSM (T42L9)

Forecast cases / date		IAPGSM3				ECGSM			
		average * *		500 hPa		average * *		500 hPa	
		TCC	RMSE	TCC	RMSE	TCC	RMSE	TCC	RMSE
Day 1	Apr.7	0.8242	33.9	0.8598	31.3	0.8093	35.5	0.8545	32.1
	June 14	0.7872	32.0	0.8358	29.9	0.7780	33.1	0.8384	30.1
	Nov.5	0.8463	37.7	0.9032	32.2	0.8423	38.6	0.8971	33.3
	Jan.23	0.8239	42.4	0.8464	38.7	0.8115	44.2	0.8395	39.4
	mean *	0.8205	36.5	0.8613	33.0	0.8103	37.9	0.8574	33.7
Day 2	Apr.7	0.8485	48.5	0.8735	45.9	0.8238	52.0	0.8500	50.9
	June 14	0.8377	41.8	0.8762	38.6	0.8172	45.6	0.8508	44.5
	Nov.5	0.8434	63.2	0.8842	56.7	0.8371	65.0	0.8787	58.0
	Jan.23	0.7732	70.3	0.7912	60.5	0.7669	71.0	0.7915	59.6
	mean *	0.8250	56.0	0.8563	50.4	0.8113	58.4	0.8428	53.3
Day 3	Apr.7	0.8045	65.2	0.8235	64.4	0.7899	68.3	0.8124	68.8
	June14	0.7511	60.1	0.7929	58.3	0.7393	63.6	0.7688	65.8
	Nov.5	0.7652	89.0	0.8113	78.8	0.7706	90.0	0.8134	79.2
	Jan.23	0.6803	105.8	0.6938	88.7	0.6511	108.7	0.6657	91.0
	mean *	0.7503	80.0	0.7804	72.6	0.7377	87.7	0.7651	76.2
Day 4	Apr.7	0.7365	84.1	0.7584	83.9	0.7255	87.8	0.7503	89.6
	June 14	0.6648	72.7	0.7293	69.2	0.6488	78.4	0.6880	80.7
	Nov.5	0.6556	113.2	0.6956	101.2	0.6621	114.3	0.7005	102.6
	Jan.23	0.6721	129.0	0.6777	108.2	0.6387	134.0	0.6511	113.6
	mean *	0.6823	99.8	0.7153	90.6	0.6688	103.6	0.6975	96.6
Day 5	Apr.7	0.6813	98.3	0.6848	101.3	0.6671	103.1	0.6765	108.3
	June 14	0.6233	77.0	0.6984	73.7	0.6112	83.9	0.6646	86.8
	Nov.5	0.5486	130.7	0.5894	115.6	0.5404	133.7	0.5886	117.5
	mean *	0.6177	102.0	0.6575	96.9	0.6062	106.9	0.6432	104.2

* for four cases.

* * Vertical average for 100, 200, 300, 500, 700 and 850 hPa.

accuracy, thus greatly enhancing the calculated accuracy of $\partial T / \partial P$, while $\partial T / \partial P$ is computed by vertical finite difference in usual spectral scheme, which often produces larger error near the tropopause. However calculated error of $\partial T / \partial P$ will become small with increasing vertical resolution.

2. *Comparison of Results for Higher Resolution T42L9*

Forecasts up to 5 days for four cases mentioned above have been carried out with T42L9 (for January 23 case, since the absence of observation data of day 5, only the verification of first four days is performed). Table 1 indicates the forecast TCC, RMSE and their mean for 4 cases with IAPGSM3 and ECGSM. As can be seen in Table 1, the forecast effect of

IAPGSM3 is better than ECGSM except for November 5 case for which both forecasts are equivalent. June 14 case is one of the better cases, TCC of day 4 at 500 hPa is 4.1% higher and RMSE 11.7 meters lower. Fig.6 shows the mean of TCC and RMSE for four cases. It can be seen that IAPGSM3 always has better prediction performance than ECGSM. Their difference is not large in the first day, but larger in other days, for example, being 1.8% for TCC at 500 hPa in day 4 and 6 meters for RMSE. For the mean of four cases, TCC of IAPGSM3 for 500 hPa is 1.3% higher than ECGSM per day, 1.2% higher for vertical average,and RMSE for both 500 hPa and vertical average is 4 meters less per day.

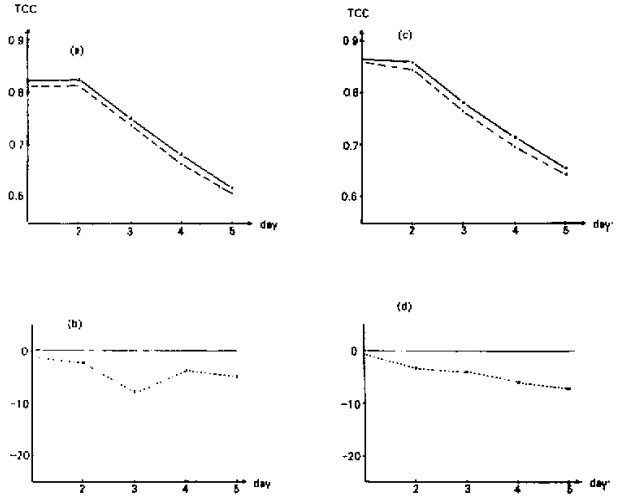

Fig.6. The mean of TCC and RMSE of four cases for IAPGSM3 and ECGSM. Vertical average: (a) TCC (b) difference of RMSE. 500 hPa: (c) TCC (d) difference of RMSE (unit: m) ——— IAPGSM3 ——— ECGSM.

Fig. 7(a) Observed 500 hPa height (June 18, 1979). (b) day 4 predicted 500 hPa height with IPAGSM3. (c) day 4 predicted 500 hPa height with ECGSM.

Next, we give an example, June 14, to illustrate the prognosis at 500 hPa. The subtropical high over the western Pacific experiences a process of strengthening and northward shifting during the prediction period, the ridge line of the high reaching north of 20°N from 15°N. The Yangtze River valley entered mei-yu period from June 18. Both IAPGSM3 and ECGSM well

predict this process, but the forecast position of subtropical high is too far to the north. Figs.7a, b, c show the 500 hPa height field of the Northern Hemisphere observed and predicted by both IAPGSM3 and ECGSM. It can be found that the position of main troughs and ridges predicted is basically coincident with the observed. However, the forecast of IPAGSM3 is closer to the observation than ECGSM in terms of the position and intensity of subtropical high. For some other systems, the foreacst of ECGSM is not as good as IPAGSM3. For example, the trough predicted by ECGSM at 90°E is too far to the south and the trough in 30–60°W is too deep. On day 5 forecast, there is a tilted shear line from the Korea Peninsula to the Yangtze River valley. The prediction of IAPGSM3 is also better than ECGSM (Fig. not shown), even though the tilt of the trough is not well captured by both.

3. *Discussion on Computational Stability*

Here we will give a brief discussion on the possible reason for computational instability when C_0 is taken as a constant. One of the advantages for hydrostatic extraction method is the indroduction of C_0, which represents the stratification $\partial\overline{T}/\partial P$ of a reference atmosphere. Utilizing (2.1)

$$\frac{\partial\overline{T}}{\partial P}=\frac{1}{P}\left(\frac{R\overline{T}}{C_p}-\frac{C_0^2}{R}\right), \tag{4.1}$$

here, knowing C_0 and $\overline{T}$, $\partial\overline{T}/\partial P$ can be calculated accurately, the computational error caused by vertical finite difference is reduced, especially near the tropopause. However, for a constant C_0, $\partial\overline{T}/\partial P$ is always larger than zero (taking derivative of (2.3)) and increases rapidly with decreasing p in the upper level. Meanwhile $\partial T'/\partial P$ becomes very large, and their signs are opposite. As a result, $\partial T/\partial P$ becomes a small residual between two large terms, which is just similar to the pressure gradient term near tilted topography on σ surface. Fig.8a shows $\partial\overline{T}/\partial P$, $\partial T'/\partial P$ *and* $\partial T/\partial P$ calculated from the initial value of June 14 case at a point A (36°N, 90°E) over the Tibetan Plateau. As shown in Fig.8a, the higher the level, the more $\partial\overline{T}/\partial P$,and$\partial T'/\partial P$ diverge and the larger the error of calculated $\partial T/\partial P$, even its sign opposite to the real. This results in that the distribution of temperature in upper layer has very large deviation from the observation. Fig.9 shows the initial temperature (June 14 case) and those obtained by integrating T21L15 to 30 hours and 31.5 hours at the point A when C_0 being constant. It can be seen that after integration of 30 hours, the temperature structure above 200 hPa, especially near the tropopause, is seriously distorted; the temperature rapidly drops near the tropopause and rapidly rises in the stratosphere. Below the tropopasue the temperature lapse rate γ is larger than γ_s, which leads to an unstable stratification. This becomes severe quickly and finally the computation breaks down. Fig.8b shows the results at point A when C_0 being $C_0(\mu,p)$. It can be found that in the upper layer, both $\partial\overline{T}/\partial P$, and $\partial T'/\partial P$ have the same sign, furthermore, $\partial\overline{T}/\partial P$ is much larger than $\partial T'/\partial P$. So a more accurate $\partial T/\partial P$ can be obtained. As is seen in Fig.2, the temperature deviation T' in the upper layer for ECGSM is very large too. Nevertheless, the scheme adopts $\overline{T}=300$ K, which increases the weight of implicit part, and due to $\partial\overline{T}/\partial P=0$, $\partial T/\partial P$ can be calculated even more accurately than by IAPGSM1 (C_0=constant) in the upper layer. Therefore the computation for scheme ECGSM is stable. It can also be seen from Fig.8b that below 200 hPa, values of $\partial T/\partial P$, calculated by scheme C_0=constant, $C_0=C_0(\mu,p)$ and ECGSM are very close to each other.

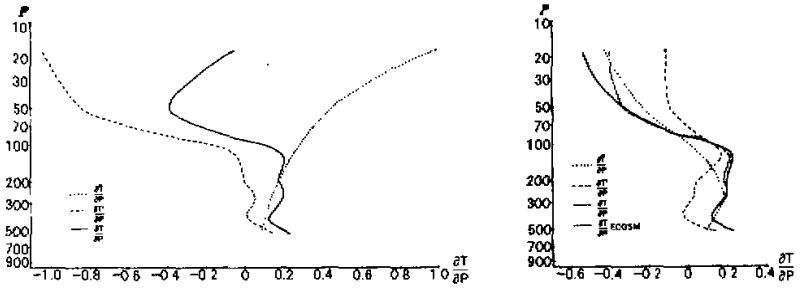

Fig.8. Variation of initial $\partial\overline{T}/\partial P$, $\partial T'/\partial P$, and $\partial T/\partial P$, with height for scheme (a) C_0=88.8 m/s, (b)$C_0 = C_0(\mu,p)$ and ECGSM at point A (36°N, 90°E), June 14 case.

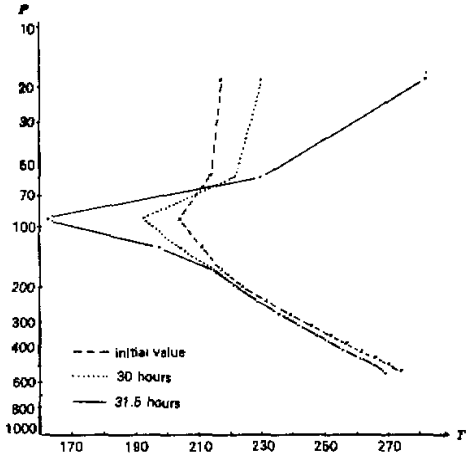

Fig.9. Vertical temperature profile of point A predicted by T21L15 at different integration time (C_0=88.8 m/s, June 14 case).

V. CONCLUSION

In this paper, various reference atmosphere of the model is discussed in detail. It shows that hydrostatic extraction scheme with constant C_0 has some advantages at low vertical resolution (T21L2,T21L5). However, as vertical resolution increases and the model atmosphere extends into the stratosphere, a constant C_0 can not properly describe the real temperature profile and even leads to computational instability. A possible reason for this is that the temperature lapse rate has a drastic change near the tropopause and serious error is apt to occur, when the vertical advection term is calculated by constant C_0.

The adoption of $C_0 = C_0(p)$ or $C_0 = C_0(\mu,p)$ not only retains the merits of the extraction scheme with constant C_0 but makes possible the accurate calculation of $\partial\overline{T}/\partial P$, and the vertical advection term, thus overcoming the above difficulties. And stable time integration and better forecast results are achieved compared with commonly used schemes.

Based on the forecast experiments for four real cases of different seasons, the scheme of

T42L9 version has gained 1.2% higher tendency correlation coefficient (or reduction of 4 meters RMS error) both for geopotential fields of 500 hPa and that averaged for 6 levels mentioned above. Synoptic evaluation also indicates a better performance in predicting the strength and location of weather systems. These preliminary results lead to the conclusion that the hydrostatic extraction scheme wth $C_0 = C_0(p)$ or $C_0 = C_0(\mu,p)$, particularly with $C_0(\mu,p)$ specified by initial fields, is practical and effective.

We are grateful to Prof. Chen et al. for origional programme of global version of T21L5 with constant C_0, and to Prof. Zhang Xuehong for many useful discussions.

REFERENCES

Baede, A. P. M. et al. (1980), Adiabatic formulation and organization of ECMWF's spectral model, ECMWF Technical Report No.15.

Chen Jiabin, Ji Liren and Wu Wanli (1987), Design and test of an improved scheme for global spectral model with reduction truncation error, *Advances in Atmospheric Sciences*, **4**: 156–168.

Simmons, A. J. et al. (1978), Stability of the semi-implicitmethod of time integration, *Mon. Wea. Rev.* **104**: 405–412.

Zeng Qingcun (1979), *Physical and mathematical fundament for numerical weather forecasting* (*in Chinese*), Science Press, 22–25, 543pp.

Zhang Xuehong (1990), Dynamical framework of IAP nine-level atmospheric general circulation model, *Advances in Atmospheric Sciences* (to be published).